Project Report for Computational Physics (Winter Term 2022/2023): Cellular Automata for Sandpiles

Anna-Maria Heyn* and Carlo Wenig†

(Dated: February 26, 2023)

From trickling grains of sand on a table and observing the development of avalanches, the criticality of such abstracted, multidimensional tables on which sand is distributed using cellular automata will be investigated. For this purpose, the critical exponents of the system will be calculated and put in relation.

Structure: In section I we will introduce the sandpile model and motivate its relevance. A theoretical introduction to the sandpile algorithm and the scaling exponents will be given in section II. Since we did many separate analyses in this project and the algorithmic part is already introduced in section II, we combined our methods and results into a single section III which is subdivided into subsections, each addressing a single subject or analysis. This way, the context of each result is clear. Finally, we will discuss our results in section IV and give a conclusion in section V.

I. INTRODUCTION: HOW SANDPILES BECOME CRITICAL AND WHY WE CARE

Why are we talking about sand? And why might this be interesting in a setting of Computational Physics? Let's start by imagining a table on which some sand is spilled. At first, not much will happen if more and more sand is added continuously. But at some point, after one too many grains, one pile will be so high that it becomes unstable and some grains will tumble down to lower points on the table. They might even fall off the table. What caused this is not necessarily the height of the pile itself, but rather the slope at some point. Only a big difference in height between some point on the table and another point close to it can cause such an avalanche. Thus, it makes sense not to look at the heights but the slopes directly and for the sake of the problem being computable, let the positions be sites on a discrete lattice. One could also put walls on the edges of the table, changing the system's boundary conditions from open to closed. Or one might even think of the behavior of the system if the grains of sand can not just tumble left, right to the front or the back, but also in fewer or more directions, corresponding to a lower or higher dimensional problem. This is where the picture of a table with sand starts to fail since it would have to grow holes and gravity would go in multiple directions, but it is nice to keep it in the back of the head for some illustrations.

An exemplary 2D sandpile that decays is shown in fig. 1. There, we can see a system where one site is disturbed and then it is relaxed until there are no more critical sites.

But this still does not explain, why we should care about this arbitrarily abstract problem. What makes this interesting is the fact that it is a study of self-organized criticality, which physicists care a lot about. Also, if one looks at the resulting pictures, one could draw analogies to self-similarity, which we will not do, but they still look nice.

The study of this problem is based on a paper of *Bak, Tang, Wiesenfeld* from 1987 which had the goal to investigate the $1/f$ noise of such systems[1]. Later, it was found that it does not show $1/f$ behavior, but further studies on the criticality were done by *Christensen, Fogedby, Jensen*[2]. The two aforementioned papers are the basis of our investigations.

To look at this problem, we first have to do some theoretical explanations of sandpiles in section II. There, we will look at a way of constructing and evolving sandpiles over time in section II A. Then, we will look at the system's scaling exponents in section II B. Those two more theoretical sections are closely analogous to the works of *Bak, Tang, Wiesenfeld*[1] and *Christensen, Fogedby, Jensen*[2]. After the theoretical introductions, we will show our results with our own new simulations in section III, discuss them in section IV and finally summarize our findings in section V.

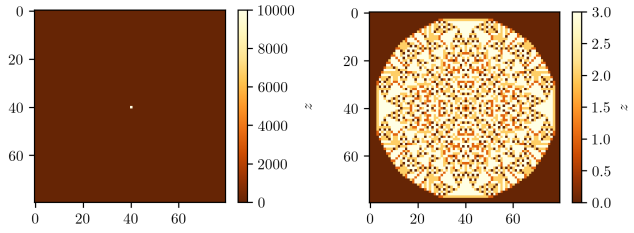

(a) Before relaxation: A *table* on which a single site has a very high slope.

(b) After full relaxation of the system. The maximum allowed slope is $z_c = 3$.

FIG. 1: A visualization of the slope of an exemplary sandpile before and after the relaxation of the full system. Different slopes are visualized by different colors.

* s6anheyn@uni-bonn.de
† s6caweni@uni-bonn.de

II. THEORY: THE SANDPILE MODEL

Before we can look at our implementation of the sandpile and its behavior, we first have to discuss how to mathematically describe it.

A. How to build a sandpile and how to let it decay

The system of the sandpile is described by a (quadratic) grid of some edge length N and some number of dimensions d. Every point r on the grid now has $2d$ neighbors and there are N^d sites on the grid. For each point, the slope $z(r)$ exists. It is defined as:

$$z(r) = h_1 + h_2 - h_3 - h_4. \tag{1}$$

Note that here h_k are the heights on the bonds between the slopes sitting on knots according to fig. 2 and that there thus is a preferred direction.

We call a point *critical*, if its slope is too high $z > z_{\text{crit}}$, where we choose $z_{\text{crit}} = 2d - 1$ to ensure that the system converges, as suggested by [2].

1. Perturbation

There are two different ways to perturb the system. The first way is similar to adding a grain of sand to a point r as shown in fig. 3. Visually, if a grain of sand is added, the height at the site changes and thus, the slope increases in one place and decreases in another (for simplicity we assume here that we only measure the slope in a favored direction of each dimension) as visualized in fig. 3b. The decrease will of course depend on the number of neighbors, i.e. the dimension of the grid. We then change the system with the *conservative* perturbing mechanism according to

$$\begin{aligned} z(r) &\to z(r) + d \\ z(r - e_i) &\to z(r - e_i) - 1 \text{ for } i = 1, ..., d, \end{aligned} \tag{2}$$

where e_i are the basis vectors of the grid. This perturbation conserves the total slope of the system. For a change of the total slope, the *non-conservative* perturbing mechanism is used:

$$z(r) \to z(r) + 1. \tag{3}$$

The differences of the two will be further discussed with our own findings in section III.

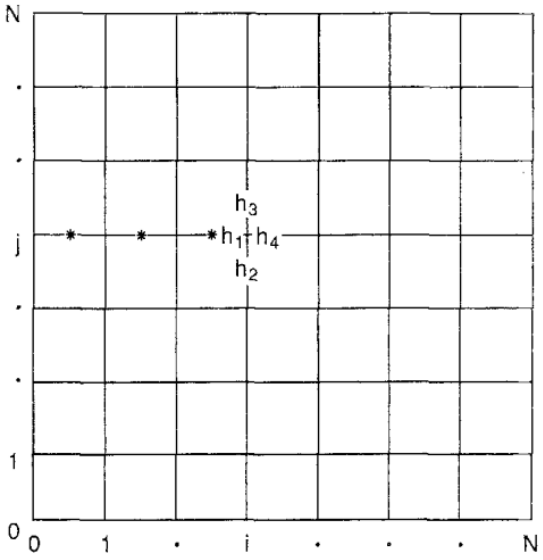

FIG. 2: A grid with the heights of the sandpile measured on the bonds, the slope can be calculated on the knots for a $N \times N$ 2D grid [2].

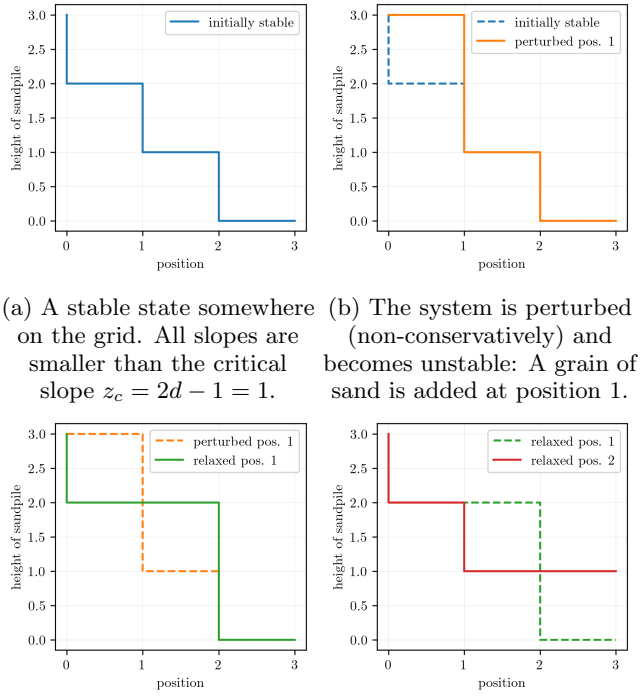

(a) A stable state somewhere on the grid. All slopes are smaller than the critical slope $z_c = 2d - 1 = 1$.

(b) The system is perturbed (non-conservatively) and becomes unstable: A grain of sand is added at position 1.

(c) Since the previous state was unstable, a grain topples down following the slope. The system is still unstable.

(d) Another grain of sand topples down. Then, since no $z > z_c$ remain, the system is stable.

FIG. 3: A visualization of an avalanche somewhere in a system. Here we chose $z_c = 2d - 1 = 1$ for the purpose of clarity in a 1D system.

2. Relaxation

If a site has a critical slope according to $z(r) > z_c$, it is unstable and needs to be relaxed.

$$\begin{aligned} z(r) &\to z(r) - 2d + (\text{no. of } r_i \text{ with } i = N-1) \\ z(r+e_i) &\to z(r+e_i) + 1 \quad \text{if } r_i \neq N-1 \\ z(r-e_i) &\to z(r-e_i) + 1 \quad \text{for } i = 1, ..., d. \end{aligned} \tag{4}$$

The actual relaxation as described by eqs. 4 provide a way of *toppling* the sandpiles. In our picture from the beginning, this corresponds to have sand grains slide down as shown in fig. 3c, resulting in a decrease of the previously (critical) site's slope while the surrounding ones of course must be increased. For more than one dimension, this means that $2d$ of the slope will be deducted from the previously critical site, while all neighbors still just gain a single unit of slope.

From this of course follows that a neighboring site could become critical and in the next step would have to be relaxed, as shown in fig. 3d. In such a way bigger avalanches can form until the whole system becomes stable, i.e. uncritical again, and the goal is then to analyze their behavior.

For relaxation we distinguish open and closed boundary conditions. Open boundaries correspond to *sand* being able to leave the system (it falls off the table), while closed boundaries will not allow that. The relaxation algorithm with open boundary conditions is then given by eq. 5. For closed boundary conditions eq. 5 is altered to eq. 6.

$$\text{open:} \quad z(r) = 0 \text{ if there exists } r_j = 0 \tag{5}$$

$$\text{closed:} \quad z(r) = 0 \text{ if there exists } r_j = 0 \text{ or } r_j = N \tag{6}$$

Here it is worth noting that for the 0-border it is always assumed that it is closed. Since the system has a preferred directions which points away from it, this mostly will not influence the system.

If we continously perturn the system at random sites, the average slope

$$\langle z \rangle = \frac{1}{N^d} \sum_r z(r)$$

converges to a stationary state. This can also be seen in fig. 4 in sec. III for our simulation. In our case, only non-conservative perturbations with open boundary conditions are used as these will grant the most successful and fast convergence while being the easiest to analyze and sufficient for our investigations. More on the convergence as well as the different boundary conditions and perturbation methods will be discussed in section III, where we can look at our own simulation's results.

B. Scaling exponents

Examining a single avalanche, one can ask the following questions: How long did it take to relax the system after it was perturbed? How big was the avalanche? How many individual sites had to be relaxed? Does this behavior converge? Are there relations?

To look at the avalanches and their behavior in more detail, we begin by defining an indicator function f for unstable slopes in eq. 7 and from it, we can then define the instantaneous dissipation rate f_α of an avalanche α in eq. 8 counting the sites which are unstable at some time step τ of the temporal evolution of the avalanche:

$$f(r, \tau) = \begin{cases} 1 & \text{if } z(r) > z_c \\ 0 & \text{else} \end{cases} \tag{7}$$

$$f_\alpha(\tau) = \sum_r f(r, \tau) \tag{8}$$

The *total dissipation* (or size) s of an avalanche which started at $\tau = 0$ (cf. eq. 9) counts how many sites have been critical over the course of the full avalanche. Note that sites could be critical and thus relaxed multiple times if neighboring relaxations increase their slope again. This will be counted multiple times in the total dissipation, so it can be a bigger than the number of sites.

An avalanche's *lifetime* t is then defined in eq. 10 as the total time steps which passed until the system is fully relaxed, i.e. no more sites are critical. Also, the last relaxation is not necessarily at the outermost point. The *spatial linear size* l as in eq. 11 is therefore defined as the maximum distance from any point of the (fully developed) avalanche to its origin r_0.

$$s = \int_0^\infty f_\alpha(\tau) \, \mathrm{d}\tau \tag{9}$$

$$t = \max\left\{\tau : f_\alpha(\tau) > 0\right\} \tag{10}$$

$$l = \max\left\{|r - r_0| : r \in \text{avalanche}, \, r_0 \text{ origin}\right\} \tag{11}$$

These three variables will be the observables of the system, in addition to the average slope.

By using the probability distributions as suggested by source [2], we arrive at the scaling exponents τ, α, λ of the problem:

$$P(S = s) \propto s^{1-\tau} \tag{12}$$

$$P(T = t) \propto t^{1-\alpha} \tag{13}$$

$$P(L = l) \propto l^{1-\lambda}. \tag{14}$$

From this, conditonal expectation values $E(X|Y = y)$ with the following proportionalities can be inferred for all observed variables $X, Y \in \{T, S, L\}$, giving rise to more scaling exponents:

$$E(S \mid T = t) \propto t^{\gamma_1} \tag{15}$$

$$E(T \mid S = s) \propto s^{\widetilde{\gamma}_1} \tag{16}$$

$$E(S \mid L = l) \propto l^{\gamma_2} \tag{17}$$

$$E(L \mid S = s) \propto s^{\widetilde{\gamma}_2} \tag{18}$$

$$E(T \mid L = l) \propto l^{\gamma_3} \tag{19}$$

$$E(L \mid T = t) \propto t^{\widetilde{\gamma}_3}. \tag{20}$$

As calculated in source [2], by comparing these results of eqs. 12 - 20, one can get the following relations between the scaling exponents:

$$\overline{\gamma}_i = \frac{1}{\gamma_i} \quad \text{for } i = 1, 2, 3 \tag{21}$$

$$\gamma_2 = \gamma_1 \cdot \gamma_3 \tag{22}$$

$$\alpha = 2 + \frac{\lambda - 2}{\gamma_3} \tag{23}$$

$$\tau = 2 + \frac{\lambda - 2}{\gamma_2}. \tag{24}$$

With our generated data, we should then be able to approximate the behavior of these conditional expectation values to obtain the scaling exponents from eqs. 12 – 20, which should then follow the relations 21 – 24. This will be done in the next section with our own simulations.

We will also look at the behavior for different dimensions d, as they each should follow these relations.

III. METHODS & RESULTS

We simulated the temporal evolution of the sandpile model on several d-dimensional lattices with side length N over n_{tot} time steps. In this section, we will first look at how well-behaved our simulations are, compare different boundary conditions and perturbation methods and then we will calculate the scaling exponents. The code we used can be found on GitHub: `https://github.com/carlowenig/CP22-23-Final-Project-Sandpiles`.

A. Convergence

The convergence of the system can be analyzed by calculating the average slope $\langle z \rangle$ at each time step. This is shown in figure 4 for open boundary conditions and non-conservative perturbations. (Different boundary conditions and perturbation methods will be compared in section III B.)

Starting from $\langle z \rangle = 0$ for the empty grid, we observe that the average slope rises about linearly until it has reached a stationary state, in which it randomly fluctuates around a constant value. Visually this corresponds to the empty grid filling up with grains of sand during which phase almost no critical slopes appear. We will call this first phase *thermalization*. Then, upon reaching the *stationary state*, the system constantly relaxes critical slopes which appear with almost every perturbation on the grid and thus, the system stays in a self-organized critical state indefinitely.

This is the relevant phase for analyzing the power law behavior of the system. The duration of the thermalization phase is roughly proportional to N^d, meaning that for larger dimensions, it grows rapidly for larger N, which has to be taken into account when choosing the number of simulation steps. This behavior can also be seen in fig. 4.

In all our simulations, the number of steps is chosen such that there are about 100,000 steps *after* thermalization which build up the data set for our further analyses.

B. Comparison of boundary conditions and perturbation methods

We now compare the behavior of the sandpile model for different boundary conditions and perturbation methods. In fig. 5, there is a comparison of the $\langle z \rangle$ evolutions for all four cases. First, we observe that in the non-conservative case, the boundary conditions do not exhibit significantly different behavior, and the system converges quite quickly. If we consider conservative perturbations and closed boundaries, the system only very slowly converges to its stationary state, compared to the non-conservative case. For open boundaries and $d = 3, 4$ this is also the case, while for $d = 2$ the system decreases its slopes indefinitely. We interpret this as the system losing more sand through its open border than is added in each perturbation. Our results agree with those of [2]. All following analyses will be done for the non-conservative case to achieve fast convergence and for open boundaries, which is a rather arbitrary choice, since the results do not differ from closed boundaries.

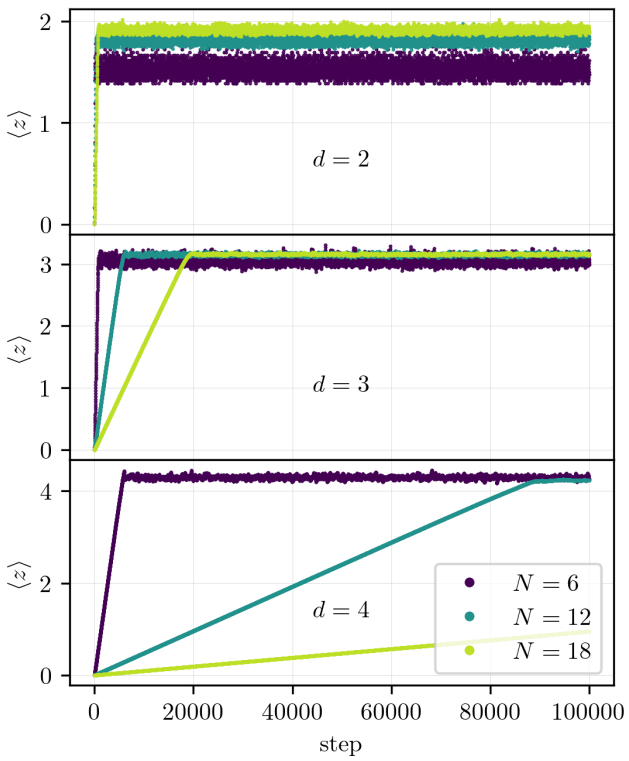

FIG. 4: Evolution of $\langle z \rangle$ in a system with open boundary conditions and non-conservative perturbations for several lattice dimensions d and sizes N. Steps are limited to 100,000.

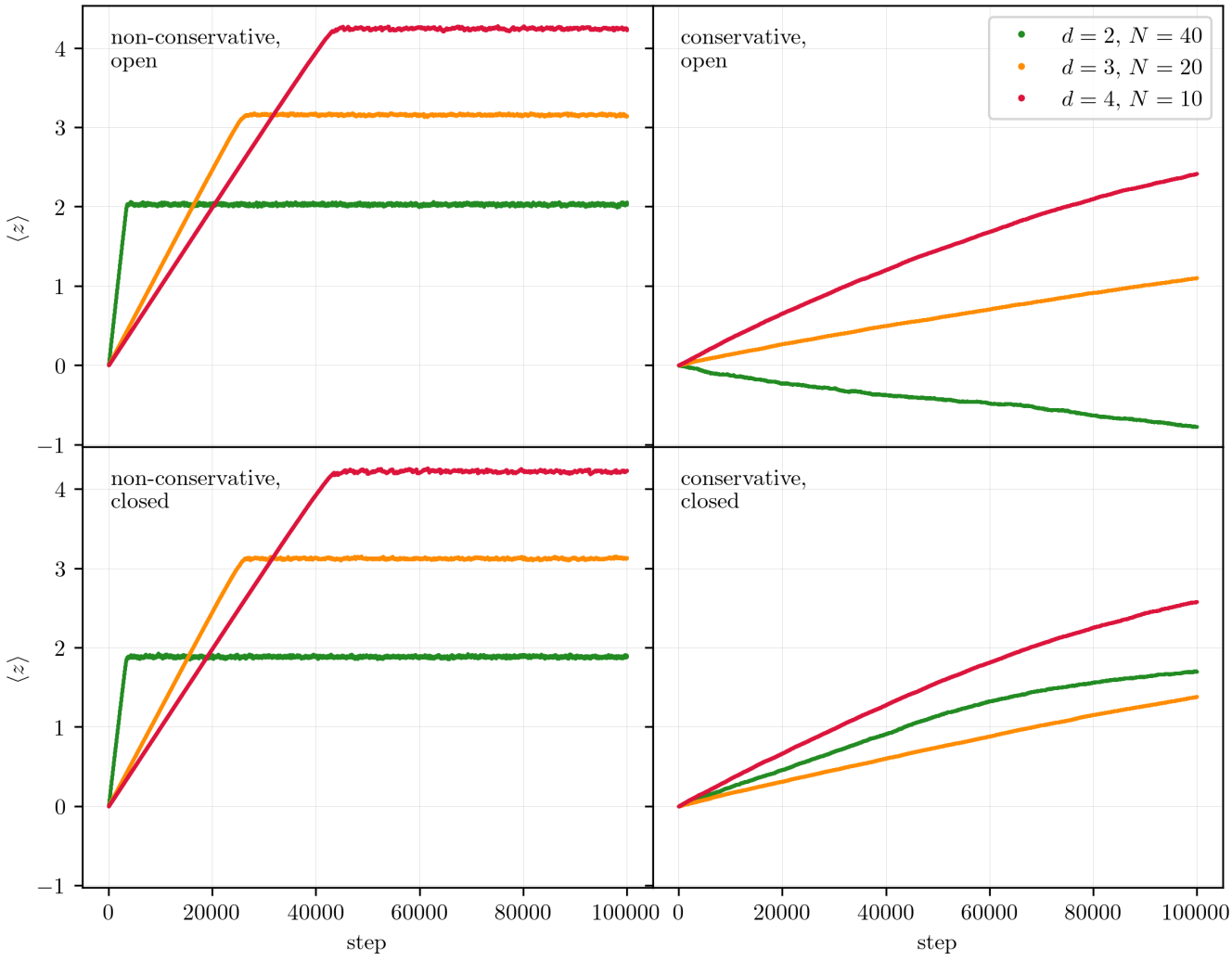

FIG. 5: Comparison of the $\langle z \rangle$ evolution between different boundary conditions and perturbation methods (conservative or non-conservative).

C. Statistical properties

After the system has thermalized and is in its stationary state, we can interpret the average slopes as variables of a statistic ensemble. In the following, we analyzed the expectation value

$$E(\langle z\rangle) = \frac{1}{n_{\text{tot}}}\sum_i \langle z\rangle_i$$

and the standard deviation

$$\sigma(\langle z\rangle) = \sqrt{\frac{1}{n_{\text{tot}}}\sum_i \Big[\langle z\rangle_i - E(\langle z\rangle)\Big]^2},$$

where the index $i = 0, 1, ..., n_{\text{tot}} - 1$ runs over all time steps of the simulation and $\langle z\rangle_i$ describes the average slope at the time step i. The results are visualized in fig. 6. One can see that the expectation values at first seem to approach the value of the dimension, but for sufficiently large N or d even succeed these. It is unclear what exact limit the expectation values converge to. The standard deviations show a power law behavior

$$\sigma(\langle z\rangle) \propto N^{\beta},$$

where the dimension-dependent exponents $\beta = \beta(d)$ are determined by linear fits in the double logarithmic graphs. The results are

$$\begin{aligned}
\beta(d=2) &= -1.017 \pm 0.004 \quad (\chi^2_{\text{red}} = 2.2\cdot 10^{-4})\\
\beta(d=3) &= -1.600 \pm 0.011 \quad (\chi^2_{\text{red}} = 9.8\cdot 10^{-4})\\
\beta(d=4) &= -2.03 \pm 0.02 \quad\;\; (\chi^2_{\text{red}} = 2.0\cdot 10^{-3}).
\end{aligned}$$

Intuitively one might expect the standard deviation to be proportional to the number of lattice sites N^d, but this seems not to be the case, although the exponents grow for higher dimensions.

Next, we will inspect the autocorrelation function of $\langle z\rangle$, which describes the correlation of two system states of our simulation results which are separated by a time step interval Δ. It is defined by

$$\begin{aligned}
C(\Delta) &:= \Big\langle \big(\langle z\rangle_i - \mu\big)\cdot\big(\langle z\rangle_{i+\Delta} - \mu\big)\Big\rangle\\
&= \frac{1}{n_{\text{tot}} - \Delta}\sum_{i=0}^{n_{\text{tot}}-1-\Delta} \big(\langle z\rangle_i - \mu\big)\big(\langle z\rangle_{i+\Delta} - \mu\big),
\end{aligned}$$

where $\mu = E(\langle z\rangle)$. The computed values for selected d and N are illustrated in fig. 7. One observes that the autocorrelation function starts from a plateau at $C(0)$, then at some d- and N-dependent point starts to decrease for growing Δ and finally fluctuates around zero. This means, that for short time intervals Δ, there exists a high correlation between the average slopes while for larger intervals there is effectively no correlation left. The high correlation at short time intervals shows that the grid will not change much if local changes at non-critical sites are made. On the other hand, if a critical site is perturbed, the avalanches can in general have large spatial sizes, therefore will alter most of the slopes on the grid and thus will change it a lot from the previous one. This then causes the correlation to drop to zero.

We will quantify the interval at which the correlation collapses by the *transition interval* Δ_{trans}, which is the point at which the autocorrelation function is reduced to at most half of its original value $C(0)$:

$$\Delta_{\text{trans}} := \min\left\{\Delta : C(\Delta) < \frac{1}{2}C(0)\right\}.$$

As can be seen in fig. 7, this transition varies depending on d and N. The exact dependence is visualized in fig. 8. We again see a power law dependence

$$\Delta_{\text{trans}} \propto N^{\delta},$$

where the exponents were evaluated by linear fits:

$$\begin{aligned}
\delta(d=2) &= 1.178 \pm 0.013 \quad (\chi^2_{\text{red}} = 2.0\cdot 10^{-3})\\
\delta(d=3) &= 1.867 \pm 0.025 \quad (\chi^2_{\text{red}} = 5.0\cdot 10^{-3})\\
\delta(d=4) &= 2.553 \pm 0.035 \quad (\chi^2_{\text{red}} = 4.7\cdot 10^{-3}).
\end{aligned}$$

The exponent δ increases by about 0.69 ± 0.05 for each added dimension, which approximately implies the following relation:

$$\Delta_{\text{trans}} \propto N^{-0.2+0.69\cdot d}.$$

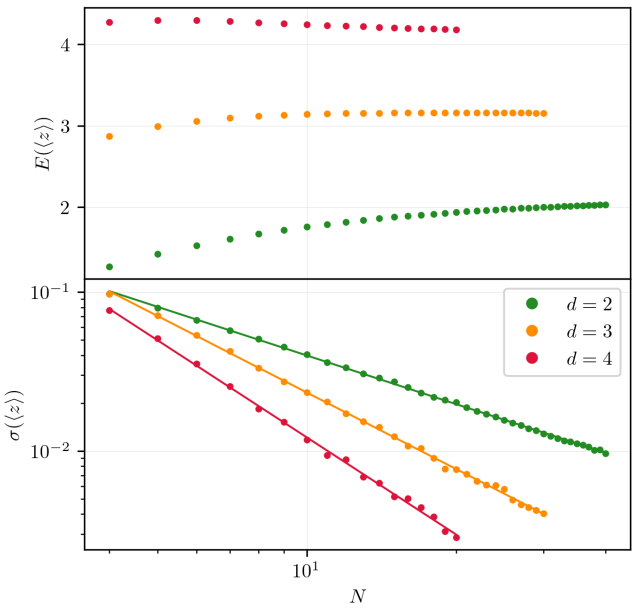

FIG. 6: Expectation values and standard deviations of the average slope in stationary states plotted against the lattice size N for different dimensions d. In the top diagram, the dimensions are marked by dashed lines for reference. In the bottom diagram, linear fits in the double logarithmic graphs are shown as solid lines.

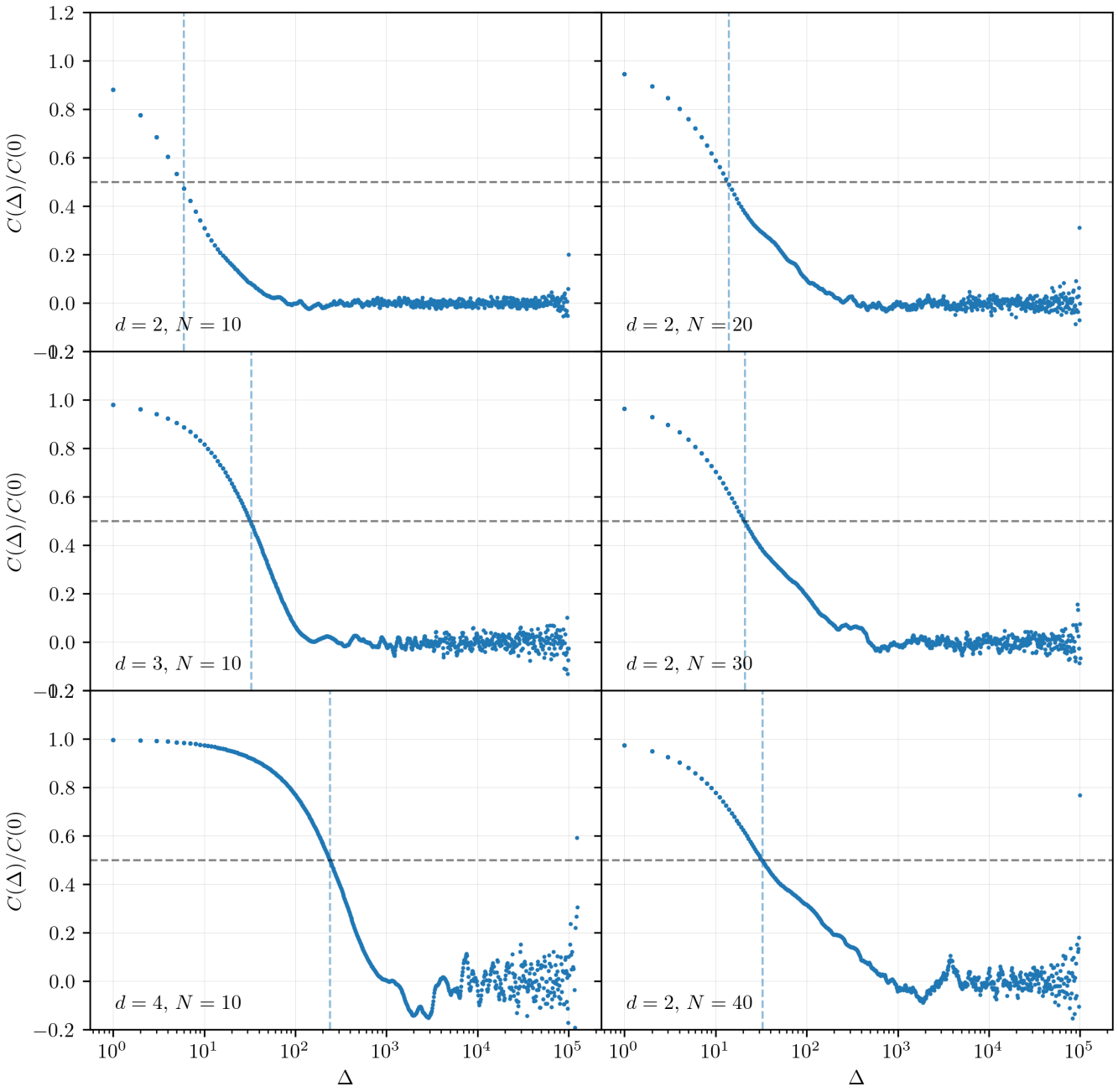

FIG. 7: Autocorrelation function of the average slope for selected lattice sizes and dimensions. Autocorrelations are normalized by the variance $V(\langle z \rangle) = C(0)$. Transition intervals Δ_{trans} with $C(\Delta_{\text{trans}}) = \frac{1}{2}C(0)$ marked by dashed lines.

It should be noted that without further analyses of different dimensions, this relation is just a rough guess for $d = 2, 3, 4$ and should not be generalized.

Also, we see in the plot that the logarithmic transition intervals are always smaller than $\log \Delta_{\text{trans}} \approx 6$, i.e. $\Delta_{\text{trans}} \approx 400$, for the cases we considered here. This interval is two to three magnitudes shorter than the total sample size of 100,000 steps. For this reason, the correlation can be neglected in our error estimation, so we do not need to perform a more sophisticated error analysis method, like for example the bootstrap method. For systems with higher-dimensional or larger lattices, this might not be the case.

D. Avalanche structure

The resulting development of avalanches can be nicely visualized for the two-dimensional case, which was done in figure 9. Since our relaxation algorithm increases the neighbor slopes in all directions, as previously mentioned, the avalanches are not restricted to "travel" continuously in a single direction, but can also visit sites they have already visited before or evolve in two separate regions simultaneously. This phenomenon can be easily seen in those avalanche plots in fig. 9. Here, the passage of time (or the number of relaxation steps already taken) is indicated by the color becoming brighter. The brightest spots are not necessarily at the outer borders of the avalanches and there sometimes is more than one bright region.

Note, that the total dissipation s is sometimes a lot bigger than the grid size of 20x20 for the example chosen in fig. 9, indicating that sites have been critical more than once, as mentioned in Section II B. The spatial linear size l always measures the maximum distance between the origin denoted by the orange cross to the avalanche's outermost point, which is the maximum distance between the cross and a site that is still colored.

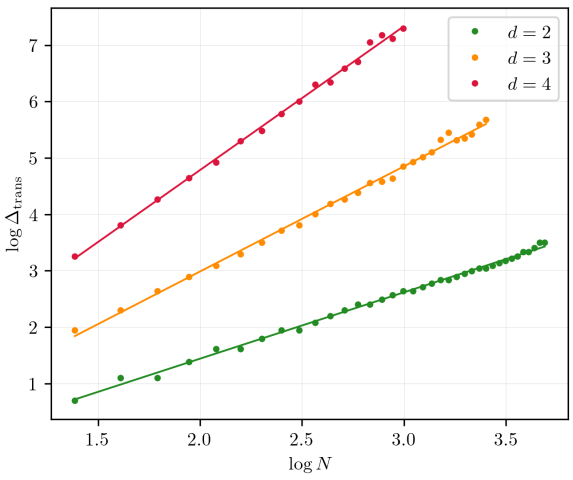

FIG. 8: Double logarithmic plot of the transition intervals Δ_{trans} as functions of N for different dimensions d. Linear fits are shown as solid lines.

E. Restrictions on the obtained data

Since the linear size L of an avalanche describes the maximum distance it "traveled" from its origin, it cannot be larger than the system size N. Additionally, if the origin is in the center of the lattice it must even be smaller than $N/2$ which is the most extreme case. If it is not in the middle, it may be larger. From these considerations, we can infer that the probability distributions for L are influenced by the lattice borders. In our fits in the following sections III F and III G, we only included $L < N/3$ to reduce these influences as much as possible, without throwing away too many data points.

In addition, for lifetimes $T \gtrapprox N$ or sizes $S \gtrapprox 2N$, we found an unexpected, nonlinear behavior, so we also constrained the fits to avalanches where $T < N, S < 2N$. Unfortunately, we cannot explain the reason for this behavior, since there is no natural limitation to the lifetime of an avalanche, as far as we know, and the intuitive natural limitation for the size would be $N^d \cdot t$ (for each step of the evolution, at maximum N^d slopes can be unstable) and thus much larger than $2N$. Finally, we also exclude $T = 1$, $S = 1$ and $L = 0$ from our fits, since these entries are no "real" avalanches, but only single perturbations without further effects.

F. Scaling exponents: α, τ, λ

For each configuration (d, n), we determined the scaling exponents α, τ and λ by fitting linear models to the double logarithmic graphs of the power laws. To be more specific, let $\varepsilon \in \{\alpha, \tau, \lambda\}$ be the scaling exponent connected to the variable $X \in \{T, S, L\}$ according to eqs. 12-20. Then, the probability P for a specific value x can be approximated by $P = n/n_{\text{tot}}$, where n is the number of avalanches where $X = x$ and n_{tot} is the total number of avalanches of the process. The probability follows the power law

$$P \propto x^{1-\varepsilon},$$

as previously mentioned in eqs. 12–14 and thus, the logarithm is given by

$$\log P = c + (1 - \varepsilon) \log x,$$

where c is a constant. Hence, by fitting a line to $\log P$ as a function of $\log x$, we can determine the scaling exponent ε. We weighted the line fit using the statistical error of $\log P$, which is determined by

$$\Delta(\log P) = \frac{\Delta P}{P}, \quad \Delta P = \frac{\Delta n}{n_{\text{tot}}}, \quad \Delta n = \sqrt{n}.$$

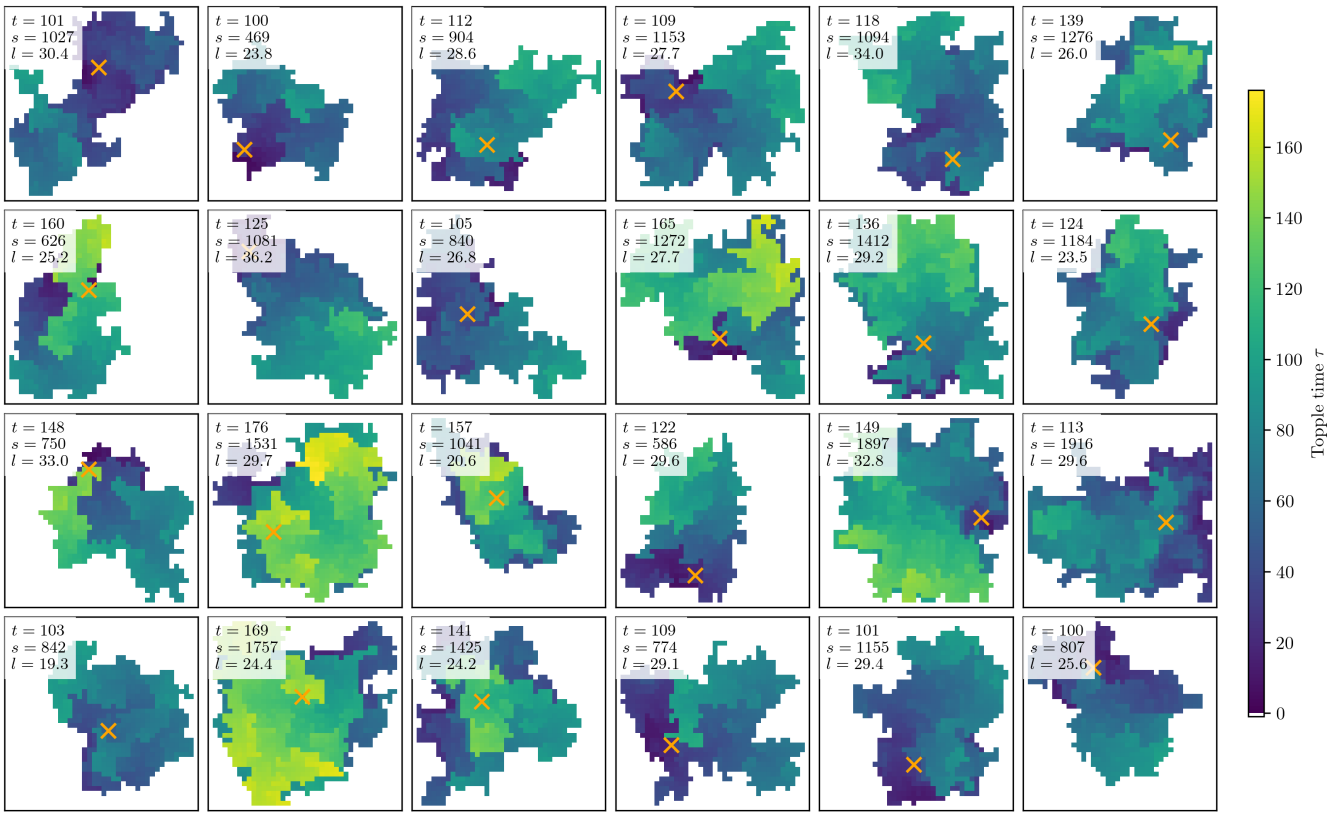

FIG. 9: Visualizations of selected avalanches with large lifetimes $t \geq 100$ for $d = 2$ and $N = 40$. Each of the 20 plots contains a single avalanche that originated from the site which is marked by the orange cross. The pixel colors represent the topple time, i.e. the time step of the avalanche evolution at which the site at that pixel was toppled (relaxed). For each avalanche, the lifetime t, the size or total dissipation s and the linear size l are given in the white box.

An illustrative example of our fit results is shown in figure 11. The fit region is restricted by the above mentioned cuts to ensure linearity of the fitted data.

Here, one can also see the behaviors described above. While the distributions for T and S show a nice linear trend in the fit region, the linear sizes L show larger fluctuations which greatly reduce the quality of the linear fit, as can also be seen from the high χ^2_{red} value. The source of these fluctuations is unclear, but one option is the hard cuts on the data we imposed. Nevertheless, we continued our investigation using these fits and keeping in mind that the values for λ might be not as representative as the other two exponents.

In figure 10 the results of the fits for the scaling exponents are shown as a function of the lattice parameters d and N. As can be seen, the exponents converge to constant limits for large lattice sizes N. The values of the parameters increase with the dimension d while they converge similarly fast for all investigated dimensions. The increase of the exponents value is due to the increase of the system's size and complexity.

The missing data points for large dimensions and lattice sizes are due to limited computing resources, while those for small lattice sizes are due to insufficient fitting data.

For selected d and N, the numeric values of the scaling exponents α, τ and λ are listed in table I. Their relations will be investigated in section IV.

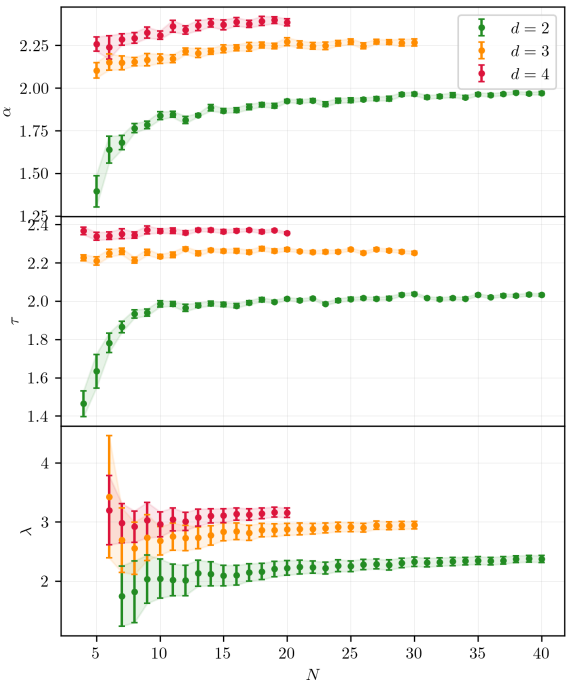

FIG. 10: Scaling exponents α, τ, λ for different lattices. Statistical errors are depicted using error bars and transparent corridors.

G. Scaling exponents: $\gamma_1, \gamma_2, \gamma_3$

Analogous to the previous section III F, for two variables $X, Y \in \{T, S, L\}$, the conditional expectation value $E(Y \mid X = x)$ for the variable Y under the condition that $X = x$ fulfills

$$E = E(Y \mid X = x) \propto x^{\gamma},$$

as given by eqs. 15–20. The logarithm is

$$\log E = c + \gamma \log x$$

where c is again a constant and $\gamma \in \{\gamma_1, \overline{\gamma}_1, \gamma_2, \overline{\gamma}_2, \gamma_3, \overline{\gamma}_3\}$ is our desired exponent.

Since the expectation values are numerically computed as mean values over all avalanches, we used the standard deviations as statistical errors. For this as well, by fitting a line to $\log E$, we can obtain the remaining exponents $\gamma_1, \overline{\gamma}_1, \gamma_2, \overline{\gamma}_2, \gamma_3, \overline{\gamma}_3$.

As an example, the data and corresponding fits for $d = 2$, $N = 40$ are illustrated in figure 12. Other (d, N) configurations we investigated, showed similar behavior. In the plots of $\log E(L \mid S = s)$ and $\log E(L \mid T = t)$ one can clearly see the impact of the lattice borders for $L > N/2 = 20$, i.e. $\log L > 3$, as discussed in section III E. Since these plots actually show deviations from linearity with higher L, the cuts we imposed are justified. This then still results in less data for the fit. The χ^2_{red} values of all the fits shown are quite low, which indicates that our statistical errors were overestimated using the standard deviation. This generalizes to different (d, N) configurations as well.

The dependence of the scaling exponents on d and N is shown in figure 13. As for the other scaling exponents, the values converge as N grows although not as quickly as before. Also, we observe that there are some bigger deviations from the line of convergence for some configurations, which probably arise from the fact, that we used a universal fit procedure for all configurations. Since there are only a few of them and they are reasonably small compared to their errors, we can still assume the model to be valid.

As we plotted both γ_i and their respective inverses, it is worth noting that the behavior of the pairs fits being the inverse of each other, although the plots do not

d	N	α	τ	λ
2	20	1.924 ± 0.009	2.012 ± 0.008	2.221 ± 0.123
2	30	1.965 ± 0.010	2.038 ± 0.007	2.326 ± 0.077
2	40	1.970 ± 0.010	2.032 ± 0.007	2.372 ± 0.057
3	20	2.272 ± 0.023	2.270 ± 0.009	2.873 ± 0.102
3	30	2.267 ± 0.020	2.252 ± 0.008	2.947 ± 0.064
4	10	2.309 ± 0.024	2.367 ± 0.011	2.958 ± 0.213
4	20	2.384 ± 0.020	2.355 ± 0.006	3.155 ± 0.080

TABLE I: Scaling exponents α, τ, λ for selected dimensions d and lattices sizes N.

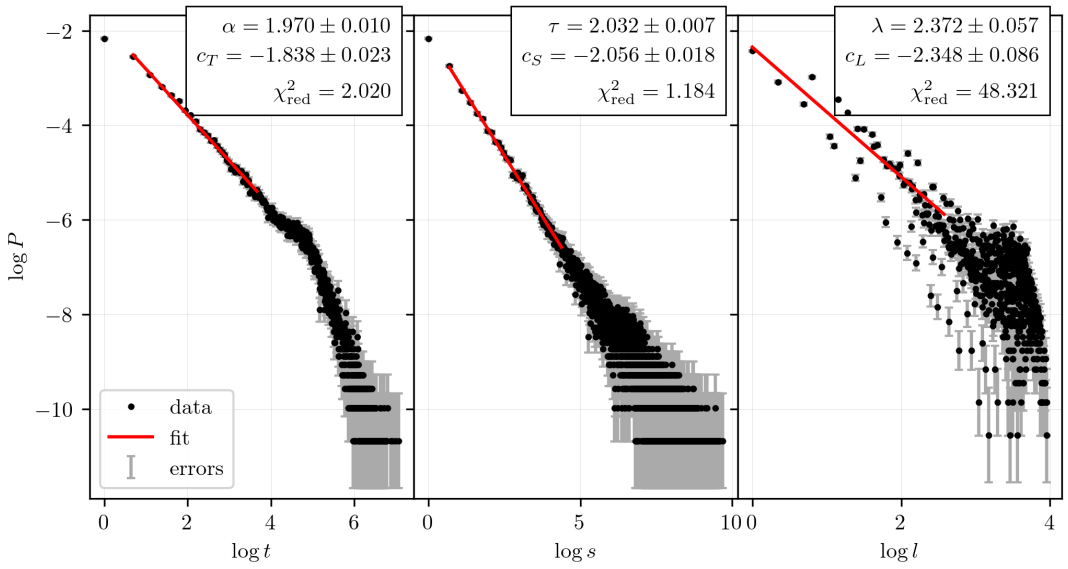

FIG. 11: Double logarithmic probability (frequency) distributions of T, S and L on a two-dimensional lattice of size $N = 40$. Shown in red are the linear fits to determine the scaling exponents α, τ and λ. The shown variables and their calculation are as explained in section III F.

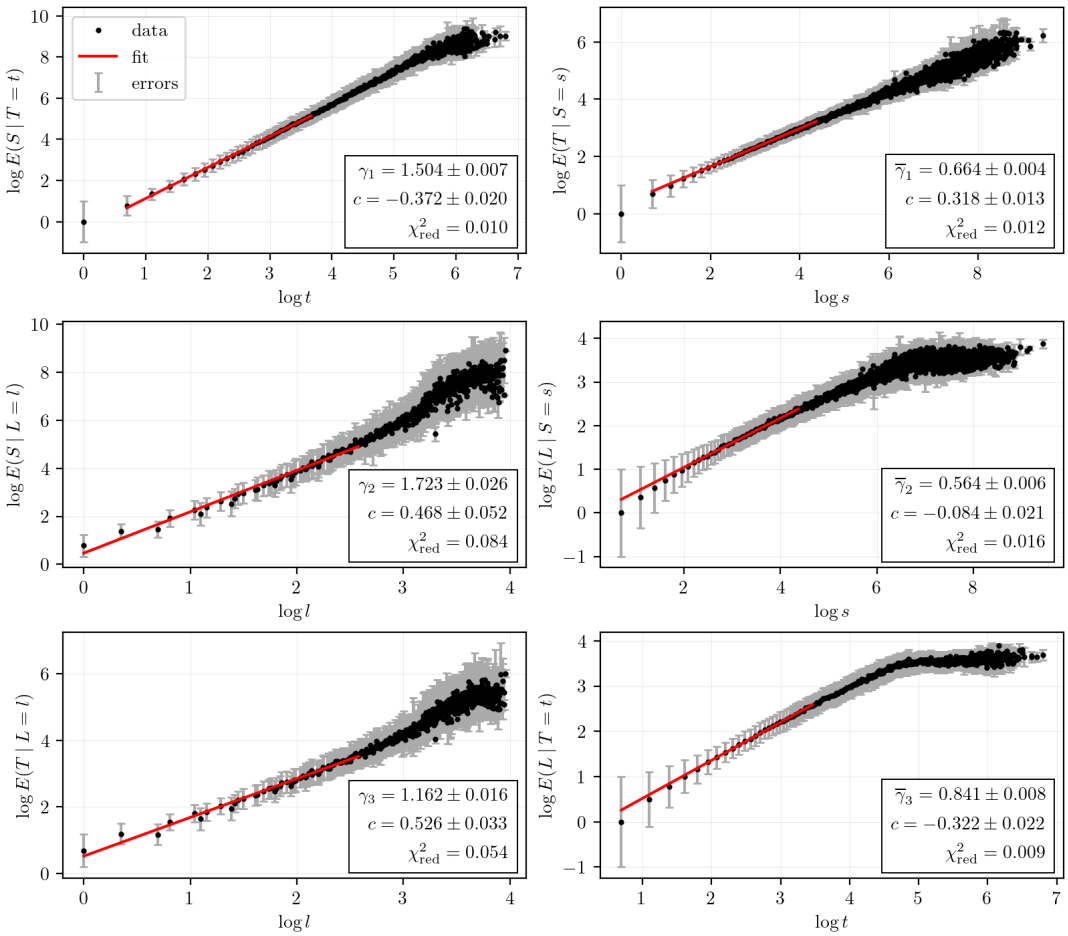

FIG. 12: Double logarithmic conditional expectation values of T, S, L on a 2D lattice of size $N = 40$. Shown in red are the linear fits to determine the scaling exponents $\gamma_i, \overline{\gamma}_i$. For the explicit calculation, see section III G.

exactly mirror each other. This might of course be due to numerical limitations since we are plotting expectation values and not direct dependencies, but it does hint at the model maybe not being able to describe the full behavior. This will be further discussed in Section IV.

In table II, the scaling exponents $\gamma_i, \overline{\gamma}_i$ are listed for a selection of lattices.

IV. DISCUSSION

With the scaling parameters obtained in the previous section, we can now test the relations 21 – 24 imposed by *Christensen, Fogedby, Jensen*[2]. For that purpose, we took the differences between the left- and right-hand sides of each of those relations to quantify the quality of agreement for each of the relations.

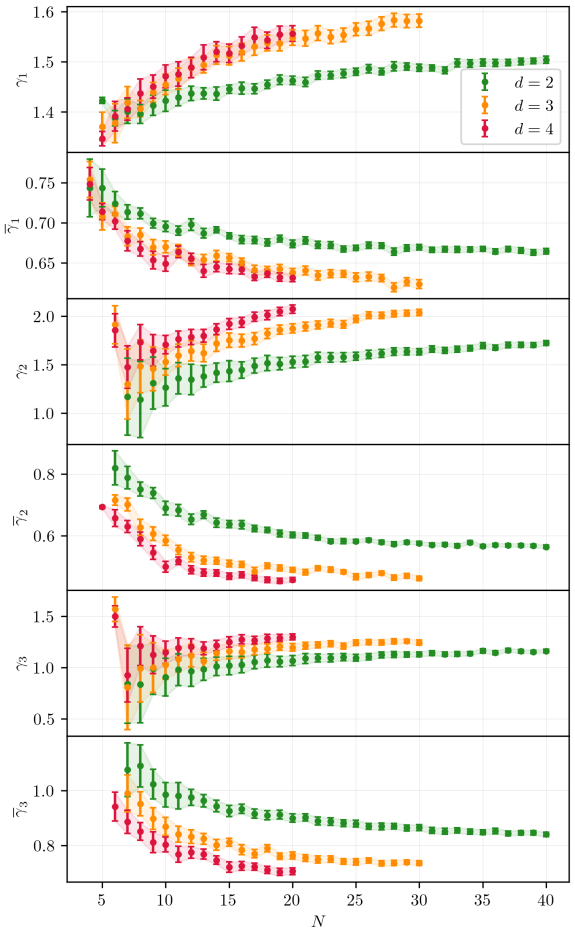

FIG. 13: Scaling exponents $\gamma_i, \overline{\gamma}_i$ for different lattices. Statistical errors are depicted using error bars and transparent corridors.

A. The γ_i exponents and their inverses

In fig. 14 the difference $\overline{\gamma}_i - 1/\gamma_i$ for $i \in \{1, 2, 3\}$ is plotted to visualize the agreement of both sides of eq. 21. There, one can see that, for all dimensions, the differences seem to converge roughly in the direction of zero with decreasing errors for growing N. The results for γ_1 (first row in fig. 14) agree well with our relations in eq. 21. For $d = 2, 3$ the differences converge to 0 within their 1σ-region, while for $d = 4$ they are still slightly below zero, which is probably because we only simulated until $N = 20$ in this case. We would expect that the 4-dimensional differences also end up at zero for sufficiently large N. The relations for γ_2 and γ_3 deviate a bit more, which is expected since their underlying expectation values do not behave as linearly as those of the γ_1 exponents, as can be seen in fig. 12.

The general behavior of the γ_i exponents indicates that for even higher lattice sizes we might also expect better numerical agreement of the expected relations 21. With more computational power available, future studies might investigate that further.

B. Relations between the different scaling exponents

For a test of relations 22, 23 and 24, the plot of the differences of both sides of the equations can be found in fig. 15. As one can see there in the first row, relation 22 is very well fulfilled for all investigated dimensions, so the relation between γ_1, γ_2 and γ_3 is confirmed. This indicates that the relations for the conditional expectation values describe the system well, although we saw some difficulties with them in Section IV A. As before, the statistical errors decrease for larger N.

d	N	γ_1	γ_2	γ_3
2	20	1.462 ± 0.009	1.527 ± 0.061	1.068 ± 0.048
2	30	1.488 ± 0.007	1.631 ± 0.033	1.129 ± 0.025
2	40	1.504 ± 0.007	1.723 ± 0.026	1.162 ± 0.016
3	20	1.548 ± 0.016	1.873 ± 0.046	1.197 ± 0.036
3	30	1.582 ± 0.013	2.037 ± 0.035	1.243 ± 0.025
4	10	1.471 ± 0.023	1.707 ± 0.095	1.149 ± 0.109
4	20	1.556 ± 0.016	2.072 ± 0.042	1.298 ± 0.029
d	N	$\overline{\gamma}_1$	$\overline{\gamma}_2$	$\overline{\gamma}_3$
2	20	0.674 ± 0.005	0.602 ± 0.009	0.900 ± 0.015
2	30	0.670 ± 0.004	0.576 ± 0.006	0.865 ± 0.011
2	40	0.664 ± 0.004	0.564 ± 0.006	0.841 ± 0.008
3	20	0.638 ± 0.005	0.489 ± 0.008	0.763 ± 0.013
3	30	0.624 ± 0.005	0.461 ± 0.007	0.736 ± 0.008
4	10	0.649 ± 0.009	0.499 ± 0.018	0.804 ± 0.027
4	20	0.632 ± 0.005	0.457 ± 0.008	0.706 ± 0.012

TABLE II: Scaling exponents $\gamma_i, \overline{\gamma}_i$ for selected dimensions d and lattices sizes N.

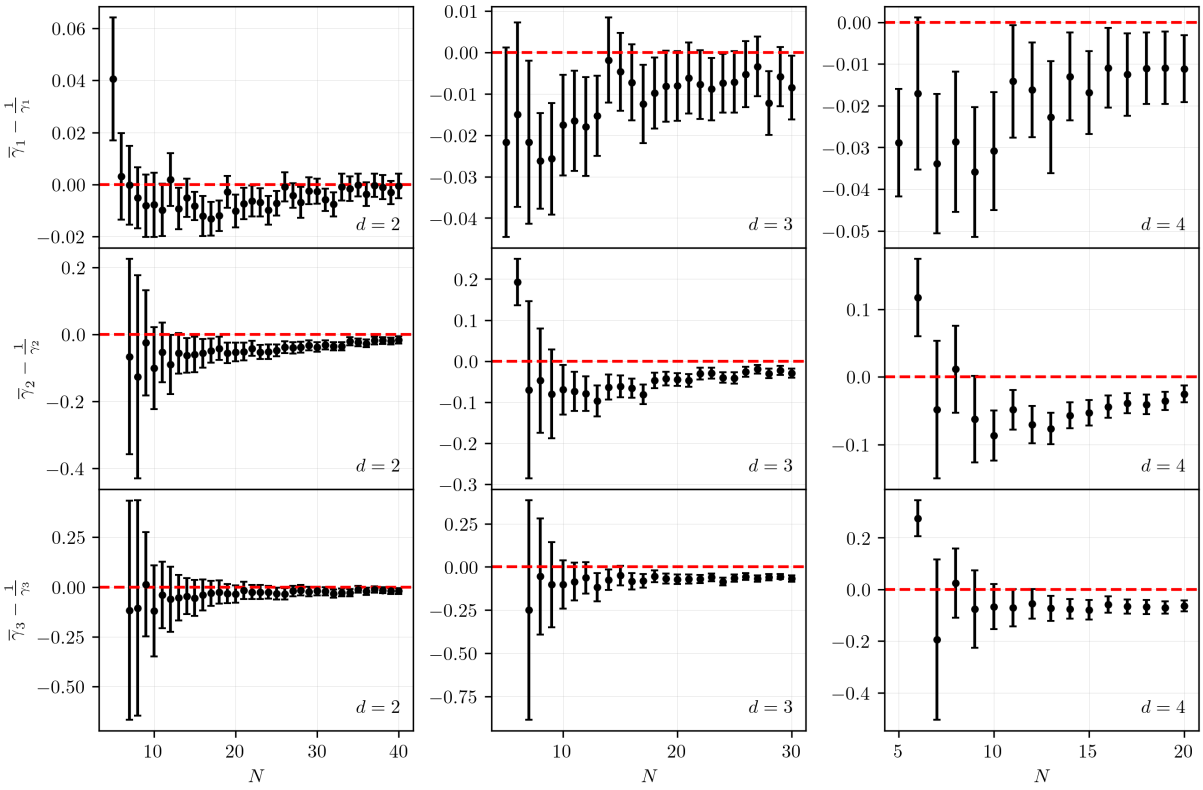

FIG. 14: Results of the fit of the scaling exponents $\gamma_1, \gamma_2, \gamma_3$ of the probability distributions from eq. 12, 13 and 13.

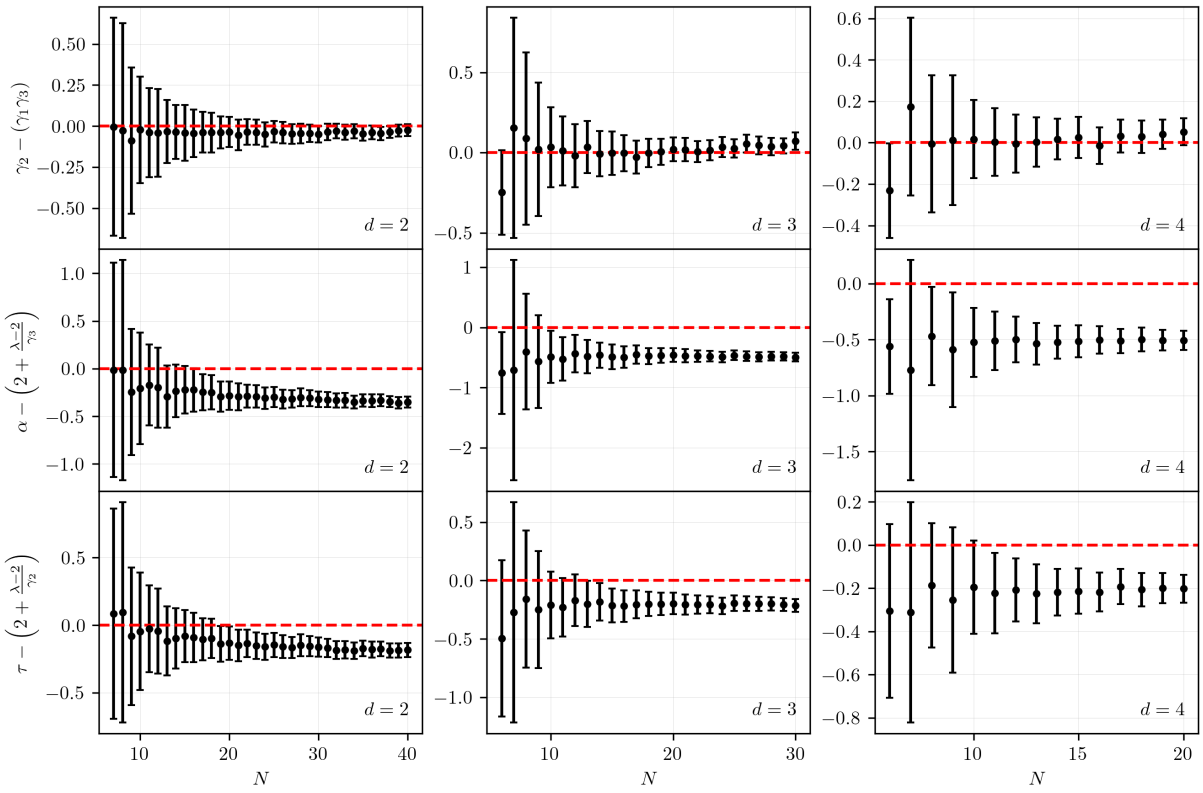

FIG. 15: Differences of the relations 22-24 for the scaling exponents $\gamma_1, \gamma_2, \gamma_3, \alpha, \tau$ and λ.

The differences for the relations 23 and 24 are not converging towards zero, but to a value slightly below zero. The observed offset cannot be attributed to the statistical errors and might be due to the imposed cuts or insufficient theoretical description of the problem. Both of them are linear in λ which we identified to be the most uncertain parameter before since it depends on the heavily fluctuating L-data the most. Therefore it makes sense, that the offset from the expectation in both cases exhibits very similar behavior. To distinguish which of the mentioned reasons is contributing more, further investigation is needed but the similarity of the behavior points in the direction of the imposed constraints for linearity in L (cf. section III E). Further investigations could look into this in more detail, especially investigating if different conditions for criticality might influence this behavior could be interesting.

V. CONCLUSIONS

In this project, we presented the results of our simulation and analysis of the self-organized criticality found in sand piles as suggested by the sources [1] and [2]. In two to four dimensions with grid sizes ranging from 4 to 40 and about 100,000 simulated time steps, we investigated the relations between the scaling exponents of the mentioned systems. The investigated scaling exponents describe the power laws followed by the probability distributions and conditional expectation values of the lifetime, spatial length and total dissipation.

Our analysis shows that the scaling exponents are mostly consistent with the theoretical predictions from the two papers. While the γ_i exponents from the probability distributions are reasonably compatible with their inverse results, the relations with the scaling exponent λ yielded an unexpected offset. Some of the deviations could be explained by considering the cuts imposed on the data to ensure linearity. To avoid such cuts, a more complex model might be needed.

Further investigation is needed to find the reason for the existing offset within the errors. Investigations of the behavior for higher dimensions or bigger lattices which would require more computational resources could also turn out to be insightful. Also, the criticality of similar systems with different conditions for criticality or slightly different ways of relaxing critical sites could be of interest to future studies. These could then also aim to explain why the observed deviations from convergence appear and why the convergence of the different exponents is different.

[1] P. Bak, C. Tang, and K. Wiesenfeld, Phys. Rev. Lett. **59**, 381 (1987), URL `https://link.aps.org/doi/10.1103/PhysRevLett.59.381`.

[2] H. J. J. K. Christensen, H.C. Fogedby, Journal of Statistical Physics **63** (1991).

LIST OF FIGURES

LIST OF TABLES